Earth and Planetary Science Letters 474 (2017) 436–446

Contents lists available at ScienceDirect

Earth and Planetary Science Letters

www.elsevier.com/locate/epsl

Regional earthquakes followed by delayed ground uplifts at Campi Flegrei Caldera, Italy: Arguments for a causal link

Matteo Lupi [a,b,*], Marcel Frehner [b], Philipp Weis [b,c], Alasdair Skelton [d], Erik H. Saenger [b,e], Nicola Tisato [b,f,g], Sebastian Geiger [h], Giovanni Chiodini [i], Thomas Driesner [b]

[a] Department of Earth Sciences, University of Geneva, Switzerland
[b] Department of Earth Sciences, ETH Zurich, Switzerland
[c] GFZ German Research Centre for Geosciences, Potsdam, Germany
[d] Department of Geological Sciences, Stockholm University, Stockholm, Sweden
[e] International Geothermal Centre, Hochschule Bochum, Bochum, Germany
[f] Dept. of Civil Engineering, University of Toronto, 35 St. George St., Toronto, Ontario M5S 1A4, Canada
[g] Department of Geological Sciences, Jackson School of Geosciences, The University of Texas at Austin, Austin, TX, USA
[h] Institute of Petroleum Engineering, Heriot-Watt University, Edinburgh, Scotland, United Kingdom
[i] Istituto Nazionale di Geofisica e Vulcanologia, Bologna, Italy

ARTICLE INFO

Article history:
Received 17 January 2017
Received in revised form 30 June 2017
Accepted 3 July 2017
Available online 26 July 2017
Editor: T.A. Mather

Keywords:
caldera
earthquakes
hydrothermal systems
delayed dynamic triggering
fluid flow
bradyseisms

ABSTRACT

Earthquake-triggered volcanic activity promoted by dynamic and static stresses are considered rare and difficult-to-capture geological processes. Calderas are ideal natural laboratories to investigate earthquake–volcano interactions due to their sensitivity to incoming seismic energy. The Campi Flegrei caldera, Italy, is one of the most monitored volcanic systems worldwide. We compare ground elevation time series at Campi Flegrei with earthquake catalogues showing that uplift events at Campi Flegrei are associated with large regional earthquakes. Such association is supported by (yet non-definitive) binomial tests. Over a 70-year time window we identify 14 uplift events, 12 of them were preceded by an earthquake, and for 8 of them the earthquake-to-uplift timespan ranges from immediate responses to 1.2 yr. Such variability in the response delay may be due to the preparedness of the system with faster responses probably occurring in periods during which the Campi Flegrei system was already in a critical state. To investigate the process that may be responsible for the proposed association we simulate the propagation of elastic waves and show that passing body waves impose high dynamic strains at the roof of the magmatic reservoir of the Campi Flegrei at about 7 km depth. This may promote a short-lived embrittlement of the magma reservoir's carapace otherwise marked by a ductile behaviour. Such failure allows magma and exsolved volatiles to be released from the magmatic reservoir. The fluids, namely exsolved volatiles and/or melts, ascend through a nominally plastic zone above the magmatic reservoir. This mechanism and the associated inherent uncertainties require further investigations but the new concept already implies that geological processes triggered by passing seismic waves may become apparent several months after passage of the seismic waves.

1. Introduction

Dynamic stresses associated with passing seismic waves generated by large earthquakes may trigger volcanic activity in the near- and in the far-field within days (Hill et al., 1995, 2002; Linde and Sacks, 1998). More recently it was shown that geological processes activated by passing seismic waves may become apparent beyond the commonly accepted time window of few days (Parsons, 2005; Jagla, 2011; Shelly et al., 2011; Watt et al., 2009; Johnson and Bürgmann, 2016). It is suggested that surface waves rather than body waves (Hill et al., 1995; Hill, 2012; Hill et al., 2002; Husen et al., 2004a, 2004b; Manga and Brodsky, 2006) are more efficient in promoting earthquake–volcano interactions. However, proposed models are still difficult to test due to the paucity of recorded triggered events (Prejean and Haney, 2014). As calderas are sensitive to incoming seismic energy (Hill et al., 1995; Husen et al., 2004a, 2004b) they are considered ideal natural laboratories to investigate earthquake–volcano interactions. Some

* Corresponding author at: Department of Earth Sciences, University of Geneva, Switzerland.
E-mail addresses: matteo.lupi@unige.ch (M. Lupi), thomas.driesner@erdw.ethz.ch (T. Driesner).

http://dx.doi.org/10.1016/j.epsl.2017.07.006
0012-821X/

magmatic systems underlying calderas periodically undergo rapid ground uplift phases (Acocella et al., 2015; Chiodini et al., 2012; Hurwitz et al., 2007; Hutnak et al., 2009; Todesco and Berrino, 2005) associated with intense local seismic activity and emission of volcanic gases marked by a strong magmatic component (Bodnar et al., 2007; Chiodini et al., 2012, 2003; Hurwitz et al., 2007; Hutnak et al., 2009; Todesco et al., 2014; Todesco and Berrino, 2005). Uplift phases (known at Campi Flegrei as bradyseismic episodes), generally followed by slow ground deflation (Del Gaudio et al., 2010), are thought to be driven by the rise of hydrothermal fluids or magmas (Battaglia et al., 2006; Bodnar et al., 2007; Chiodini et al., 2003; De Natale et al., 2006).

The Campi Flegrei caldera near Naples, Italy, is characterised by frequent bradyseismic episodes that may reach vertical ground displacement rates of about 1 m/yr (Del Gaudio et al., 2010). Most models relate bradyseismic episodes to the pressurization of the shallow hydrothermal system by injection of deep fluids (Battaglia et al., 2006; Bodnar et al., 2007; Chiodini et al., 2012; Hurwitz et al., 2007; Hutnak et al., 2009) while others invoke the intrusion of magma at shallow depths (Amoruso et al., 2014; Macedonio, 2014; Woo and Kilburn, 2010). Numerical modelling (Todesco and Berrino, 2005; Hurwitz et al., 2007; Hutnak et al., 2009; Chiodini et al., 2012) in agreement with measured fumarole gas signatures (Chiodini et al., 2003, 2012, 2016) suggests that CO_2-rich fluids would be particularly efficient in generating the observed uplifts. Previous studies suggest that these fluids are released by a cooling magmatic body at ca. 6–7 km depth (Bodnar et al., 2007; Zollo et al., 2008) and accumulate beneath a low-permeability layer at ca. 3 km depth from which they are then episodically discharged.

In spite of longstanding scientific efforts, a consistent and predictive model accounting for different geological processes at Campi Flegrei is still lacking. By combining analysis of uplift time series, statistical studies and forward simulations of seismic waves, we show evidence for an association between regional earthquakes and bradyseismic episodes. We then develop a mechanistic explanation for a causal link between regional earthquakes and ground uplift that integrates several of the above-mentioned aspects into a single coherent model. Most notably, our mechanism is compatible with the two scenarios suggesting the release of CO_2-rich brines or the intrusion of magma at shallow depths as the driving force of the bradyseismic episodes.

2. Observations

Since 1905 two distinct phases of ground deformation can be recognised at Campi Flegrei (Del Gaudio et al., 2010; De Martino et al., 2014): an overall deflation from 1905 to 1945 (not shown here) recorded by relatively sparse measurements (intervals of several years, refer to Del Gaudio et al. (2010) and De Martino et al. (2014) for the entire time sequence), and an overall inflation from 1945 to present (recorded by more frequent measurements after 1980).

To investigate potential earthquake–volcano interactions, namely dynamic triggering (that we define as a measured response of a given geological system caused by external forcing) we analysed inflation and deflation episodes for the period from 1945 to present. We find that phases of accelerated uplift may be preceded by large- to middle-size regional earthquakes (Fig. 1). This temporal association is most pronounced for the major uplift (UL) or decelerated deflation (DL) phases starting in 1950 (UL-1), 1967 (UL-3) and 1981 (UL-7). For example, the UL-7 uplift episode (characterised by ca. 1 m/yr uplift rate) started approximately 10 months after the M_w 6.9 Irpinia earthquake in 1980. Also, a more recent and major uplift episode (UL-13) began in early 2010, 11 months after the M_w 6.3 L'Aquila earthquake in 2009 (Fig. 1). Non-peer reviewed data seem to suggest that the Campi Flegrei is sensitive to passing seismic waves released by the three most recent regional earthquakes that occurred in Italy in the last decade (i.e., M_w 6.3 L'Aquila in 2009, M_w 6.2 Amatrice in 2016, M_w 6.5 Norcia in 2016). Sansivero et al. (2012) observed marked temperature variations by means of thermal camera at the Solfatara (one of the several craters of the Campi Flegrei) following the M_w 6.3 L'Aquila earthquake (Fig. 2a). Furthermore, a report of the Vesuvian Observatory (available at INGV's website) mentions that, *verbatim: "The borehole tilt station ECO recorded a permanent tilt of 0.65 μ in the E direction during the M_w 6.2 Amatrice, Italy, earthquake occurred on the 24th of August 2016 and a tilt of 0.17 μ over 19 min in the WNW direction during the M_w 6.1 Norcia, Italy, earthquake on the 26th of October 2016"*, (INGV October Report, 2016). Additionally, the INGV November Report (2016) shows that the seismic activity increased remarkably immediately after the M_w 6.5 Norcia earthquake on the 30th of October 2016 (Fig. 2b). Unfortunately, we are not able to document additional quasi-immediate responses of the Campi Flegrei to regional seismic events occurred before 2009. However, Gresse et al. (2016) point out that Campi Flegrei is sensitive to passing seismic waves and document that small transient dynamic stresses induce marked changes in CO_2 degassing.

3. Data

Sparse observations are often too descriptive and not rigorous enough to establish a causative relationship between earthquakes and response of the Campi Flegrei to external forcing. To investigate the possible association between earthquakes and bradyseismic episodes we first compared the ground elevation dataset (Del Gaudio et al., 2010; De Martino et al., 2014) at Campi Flegrei with earthquake archives (Fig. 1c). For the construction of the surface elevation curve of Fig. 1c we combined two datasets at the reference point 25A in Campi Flegrei: the first is a reconstruction of the elevation curve from 1945 to 2010 (Del Gaudio et al., 2010); the second is derived from GPS measurements between 2000 and 2015 (De Martino et al., 2014). Because the latter has a much shorter time increment than the former, we smoothed its short-period oscillations. In particular, we created a common time vector using the 7-days time increment of the GPS dataset and mapped the elevation dataset onto this common time vector. Finally, from the combined dataset we calculated a 1-yr moving average to obtain the 1945–2015 elevation curve shown in Fig. 1c. Watt et al. (2009) discuss the effects of the duration of the selected time-window when sampling datasets. In this study we used a 1-yr moving average as the preliminary inspection of the dataset (Table 1 and Fig. S1) suggests a time-lag in the order of 1 yr. Since the focus of our work is on long-term effects using a 1-yr moving average allowed us to exclude short time-scale oscillations present in the GPS data (De Martino et al., 2014). This may have hampered the capability of capturing small-scale vertical ground variations possibly triggered by weaker dynamic stresses but allowed us to focus on the effects of major seismic events only.

Next, we compiled a list of all regional earthquakes since 1945 that were larger than M_w 4.5 and closer than 300 km to Campi Flegrei (Fig. 1a) and all teleseismic (i.e., worldwide, Fig. 1b) earthquakes that were larger than M_w 6.5. To compare the effects of regional and teleseismic earthquakes at Campi Flegrei we calculated the peak ground velocity (PGV) imposed by each of these regional and teleseismic earthquakes at Campi Flegrei as a proxy for their mechanical impact on the caldera. To quantify the predicted PGV we used ground motion prediction equations. For the regional earthquakes we used an equation derived from the Italian strong motion database (Bindi et al., 2011) assuming that the site amplification effect for the reference station inside the Campi Flegrei caldera (40.82750°N, 14.1443°E) is class B (meaning that the shear wave velocities between 0 and 30 m depth range be-

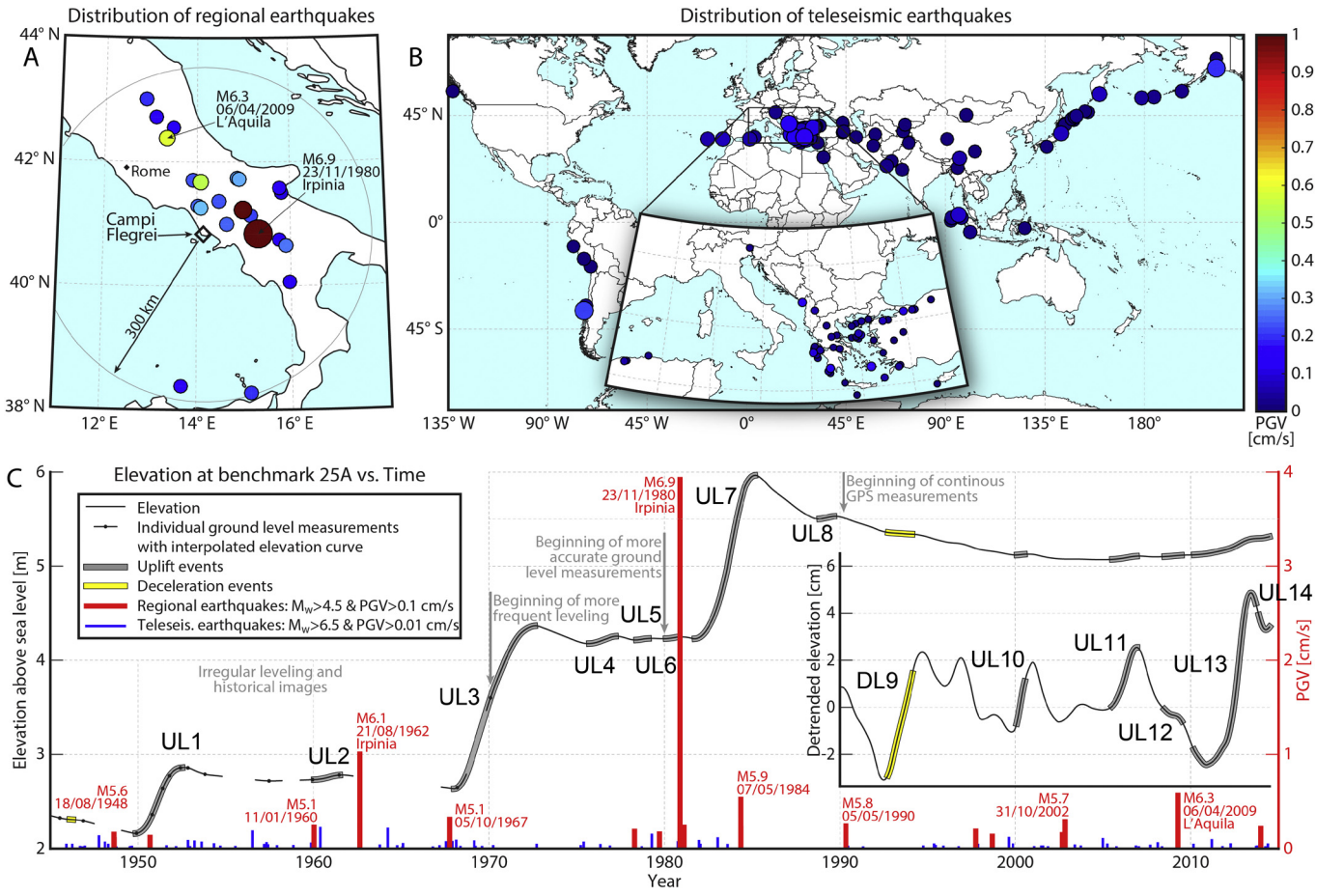

Fig. 1. Earthquake catalogue and uplift data used in the study. A) Geographic distribution of regional and B) teleseismic earthquakes. Colour-coding refers to imposed PGV at Campi Flegrei. C) One-year moving average of the ground elevation measured at the reference point 25A at Campi Flegrei and time distribution of earthquakes from 1945 to present (adapted from Del Gaudio et al., 2010 and De Martino et al., 2014). The height of the bars represents the calculated PGV at Campi Flegrei. The inset in C shows the elevation curve for the 1990 to present period de-trended using the best-fitting sine curve. The earthquake dataset is publically available and can be retrieved from the Italian earthquake catalogue from 1945 to 2006 (Mele et al., 2007) and from the EMSC website from 2006 to present for the regional earthquakes and from the cached version of the USGS earthquake archive for the teleseismic earthquakes from 1945 to 2015. (For interpretation of the references to colour in this figure, the reader is referred to the web version of this article.)

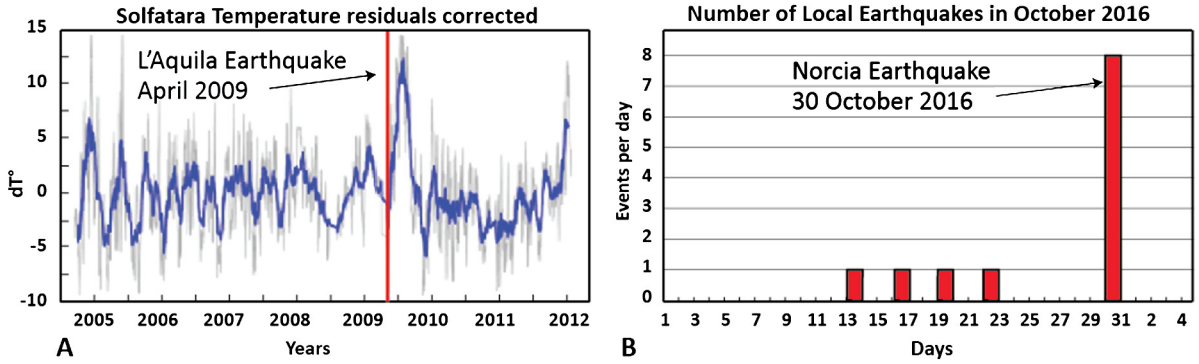

Fig. 2. Effects of regional earthquakes at Campi Flegrei. A) Chronograms of the maximum InfraRed temperature variations of the whole scene of the Solfatara after temperature residuals seasonal cyclicity removal – sky excluded (modified after Sansivero et al., 2012). Note the sharp peak after the M_w6.3 L'Aquila earthquake. B) Number of local seismic events recorded at Campi Flegrei during October 2016. Note the increase on the 30th of October 2016, the day of the M_w6.5 Norcia earthquake.

tween 360 and 800 m/s). The coefficient C_j is the same for the entire catalogue, i.e., it is assumed as the average value obtained for different frequencies. Finally, we corrected for fault mechanisms for earthquakes from 1979 to 2015 and no focal mechanism was found for the M_w6.6 earthquake in 1978. However, correction for the focal mechanism does not affect the estimate of PGV for the scope of our work (i.e. it affects the third digit after the comma).

For teleseismic earthquakes we used a similar approach (Agnew and Wyatt, 2014) valid for teleseismic distances (between 500 km and 16000 km) and magnitudes $6.5 \leq M_w \leq 9.0$. The equation estimates the maximum strain (ε) imposed by passing surface waves. As suggested by Manga et al. (2009) we approximate PGV $\simeq \varepsilon V_s$, with V_s being the shear wave velocity fixed at 2500 m/s for the shallow part of the upper crust. It must be noticed that the equation to estimate the PGV for teleseismic earthquakes was de-

Table 1

Summary of major regional events of our catalogue in relation to bradyseismic episodes. Grey bars indicate each uplift period and show the beginning, the peak, and the end of the period. M_w is the moment magnitude and FM is the focal mechanism, where N, SS, R, and U, stand for normal, strike slip, reverse, and unknown, respectively. UL stands for uplift and DL for deceleration. The first panel of the table considers all the events with PGV greater than 0.1 cm/s that can be retrieved from the catalogues. Seismic events are progressively excluded from the first and second panel to obtain the third panel of the table that shows the seismic events (i.e., the main shocks) used to conduct the statistical study. The colour coding indicates the criteria used to exclude the seismic event.

ALL REGIONAL EARTHQUAKES WITH PGV>0.1

All Regional events PGV>0.1 + Aftershocks

EQ ranked on PGV	Date	M_w	Dist	PGV
EQ 20	1948.633	5.6	157.83	0.17
EQ 32	1948.641	5.4	157.48	0.11
UL1 - 1949.816 - 1951.080 - 1952.518				
EQ 30	1950.302	4.4	41.68	0.12
EQ 27	1950.680	5.6	199.5	0.13
EQ 12	1960.030	5.0	52.36	0.24
UL2 - 1960.050 - 1960.931 - 1961.506				
EQ 2	1962.641	6.1	81.27	1.02
EQ 5	1962.641	5.7	80.06	0.48
EQ 16	1962.641	5.4	88.44	0.21
EQ 6	1967.764	5.1	47.43	0.32
EQ 7	1968.041	6.3	355.8	0.31
UL3 - 1968.052 - 1969.000 1972.603				
UL4 - 1975.458 - 1976.359 - 1977.221				
EQ 11	1976.350	6.4	607.5	0.24
EQ 18	1978.291	6.1	296.4	0.20
UL5 - 1978.401 - 1978.620 - 1979.100				
EQ 19	1979.719	5.8	227.8	0.17
UL6 - 1980.096 - 1980.537 - 1980.844				
EQ 1	1980.896	6.9	95.81	3.93
EQ 33	1980.899	5.1	94.58	0.10
EQ 21	1980.902	5.4	111.8	0.17
EQ 29	1981.044	5.2	109.1	0.12
EQ 13	1981.122	4.9	43.96	0.24
UL7 - 1981.744 - 1983.642 - 1985.155				
EQ 4	1984.352	5.9	93.63	0.54
EQ 15	1984.363	5.5	100.2	0.23
UL8 - 1988.854 - 1989.391 - 1989.909				
EQ 10	1990.347	5.8	147.6	0.25
EQ 24	1990.347	5.5	134.8	0.14
DL9 - 1992.764 - 1994.106 - 1994.106				
EQ 17	1997.738	6.0	265.5	0.20
EQ 25	1998.691	5.6	174.9	0.14
UL10 - 1999.9701- 2000.296 - 2000.583				
EQ 23	1999.775	3.8	20.05	0.16
EQ 22	2002.683	5.9	275.2	0.16
EQ 8	2002.835	5.7	116.9	0.30
EQ 9	2002.836	5.7	117.1	0.29
EQ 26	2005.391	4.4	36.07	0.14
UL11 - 2005.528 - 2006.333 - 2006.908				
UL12 - 2008.518 - 2008.9978 - 2009.476				
EQ 3	2009.266	6.3	185.7	0.58
EQ 28	2009.269	5.6	175.0	0.13
UL13 - 2010.204 - 2012.792 - 2013.692				
EQ 31	2012.388	6.1	510.8	0.11
EQ 14	2013.996	5.2	65.54	0.23
UL14 - 2014.0082				

ALL (AFTERSHOCKS AND PGV VALUES NOT CORRECTED FOR FOCAL MECHANISMS)

Regional events with PGV>0.1 Cleaned for M_w and Dist

EQ ranked o PGV	Date	M_w	Dist	PGV
EQ 20	1948.633	5.6	157.83	0.17
EQ 32	1948.641	5.4	157.48	0.11
UL1 - 1949.816 - 1951.080 - 1952.518				
EQ 27	1950.680	5.6	199.53	0.13
EQ 12	1960.030	5.0	52.36	0.24
UL2 - 1960.050 - 1960.931 - 1961.506				
EQ 2	1962.641	6.1	81.27	1.02
EQ 5	1962.641	5.7	80.06	0.48
EQ 16	1962.641	5.3	88.44	0.21
EQ 6	1967.764	5.1	47.43	0.32
UL3 - 1968.052 - 1969.000 1972.603				
UL4 - 1975.458 - 1976.359 - 1977.221				
EQ 18	1978.291	6.1	296.45	0.20
UL5 - 1978.401 - 1978.620 - 1979.100				
EQ 19	1979.719	5.8	227.80	0.17
UL6 - 1980.096 - 1980.537 - 1980.844				
EQ 1	1980.896	6.9	95.81	3.93
EQ 33	1980.899	5.1	94.58	0.10
EQ 21	1980.902	5.4	111.83	0.17
EQ 29	1981.044	5.2	109.10	0.12
EQ 13	1981.122	4.9	43.96	0.24
UL7 - 1981.744 - 1983.642 - 1985.155				
EQ 4	1984.352	5.9	93.63	0.54
EQ 15	1984.363	5.5	100.21	0.23
UL8 - 1988.854 - 1989.391 - 1989.909				
EQ 10	1990.347	5.8	147.66	0.25
EQ 24	1990.347	5.5	134.81	0.14
DL9 - 1992.764 - 1994.106 - 1994.106				
EQ 17	1997.738	6.0	265.56	0.20
EQ 25	1998.691	5.6	174.94	0.14
UL10 - 1999.9701- 2000.296 - 2000.583				
EQ 22	2002.683	5.9	275.26	0.16
EQ 8	2002.835	5.7	116.94	0.30
EQ 9	2002.836	5.7	117.16	0.29
UL11 - 2005.528 - 2006.333 - 2006.908				
UL12 - 2008.518 - 2008.9978 - 2009.476				
EQ 3	2009.266	6.3	185.74	0.58
EQ 28	2009.269	5.6	175.05	0.13
UL13 - 2010.204 - 2012.792 - 2013.692				
EQ 14	2013.996	5.2	65.54	0.23
UL14 - 2014.0082				

EARTHQUAKES USED IN THE STATISTICAL STUDY

Regional events with PGV>0.1 cleaned for M_w and Dist and No Aftershocks, after correction for focal mechanisms

EQ ranked on PGV	Date	M_w	Dist	PGV – corrected
EQ 20-U	1948.633	5.6	157.83	0.17
UL1 - 1949.816 - 1951.080 - 1952.518				
EQ 27-U	1950.680	5.6	199.53	0.13
EQ 12-U	1960.030	5.0	52.36	0.24
UL2 - 1960.050 - 1960.931 - 1961.506				
EQ 2-U	1962.641	6.1	81.27	1.02
EQ 6-U	1967.764	5.1	47.43	0.32
UL3 - 1968.052 - 1969.000 1972.603				
UL4 - 1975.458 - 1976.359 - 1977.221				
EQ 18-U	1978.291	6.1	296.45	0.20
UL5 - 1978.401 - 1978.620 - 1979.100				
EQ 19-N	1979.719	5.8 6	227.80	0.17
UL6 - 1980.096 - 1980.537 - 1980.844				
EQ 1-N	1980.896	6.9	95.81	3.93
EQ 13-N	1981.122	4.9	43.96	0.24
UL7 - 1981.744 - 1983.642 - 1985.155				
EQ 4-N	1984.352	5.9	93.63	0.54
UL8 - 1988.854 - 1989.391 - 1989.909				
EQ 10-SS	1990.347	5.8	147.66	0.25
DL9 - 1992.764 - 1994.106 - 1994.106				
EQ 17-N	1997.738	6.0	265.56	0.20
UL10 - 1999.9701- 2000.296 - 2000.583				
EQ 22-SS	2002.683	5.9	275.26	0.16
EQ 8-SS	2002.835	5.7	116.94	0.30
UL11 - 2005.528 - 2006.333 - 2006.908				
UL12 - 2008.518 - 2008.9978 - 2009.476				
EQ 3-N	2009.266	6.3	185.74	0.58
UL13 - 2010.204 - 2012.792 - 2013.692				
EQ 14-N	2013.996	5.2	65.54	0.23
UL14 - 2014.008 - still ongoing				

Removed because:

- Below M_w4.5
- Further than 300 km threshold
- Aftershock of same seismic sequence (kept the one with larger PGV)
- Removed after fault correction - below 0.1 PGV cm/s

rived for California (Agnew and Wyatt, 2014) and to the best of our knowledge, no regression equation for teleseismic and large-magnitude events has been published for Italy. To obtain realistic PGV results we calibrated V_s until the estimated PGV using the formula of Agnew and Wyatt (2014) fits the measured PGV values at the reference station to one decimal place. More specifically, we calibrated our estimated PGV values according to measured PGV values imposed by recent major earthquakes (e.g., M_w 9.1 Sumatra (2004), M_w 8.8 Maule (2010), M_w 9.0 Tohoku (2011), and M_w 7.1 Van (2011)) recorded at publically accessible INGV seismic stations nearby Campi Flegrei.

Our observations rely on the criteria used to determine uplift events. To the best of our knowledge a quantitative description of bradyseismic events does not exist in the literature. Hence, we fit data-driven observations with a quantitative definition of bradyseismic events. Here we define bradyseismic episodes based on two criteria: either i) the uplift rate is larger than 1 cm/yr (uplift episodes – UL, shaded grey in Fig. 1c) or ii) the uplift rate is 3 cm/yr faster than the average uplift rate of the preceding 3 yr (decelerated deflation – DL, shaded yellow in Fig. 1c). Based on a qualitative inspection of the data we infer that 12 bradyseismic episodes were preceded by a regional earthquake with an estimated PGV above 0.1 cm/s (see column 3 of Table 1). Only two uplift episodes (UL-4 and UL-12) were not preceded by an earthquake with PGV $>$ 0.1 cm/s. The corollary that regional earthquakes with PGV $>$ 0.1 cm/s are followed by uplift episodes appears to hold for most of these earthquakes (Table 1).

Before 1980, ground elevation measurements are sparse but still allow us to constrain the onset of uplift episodes. Almost all the earthquakes with PGV $>$ 0.1 cm/s during this time period were followed by a ground level measurement, confirming an on-going

deflation before the onset of a new uplift episode. The one exception is the M_W 6.1 Irpinia earthquake in 1962. We were unable to verify whether this earthquake was followed by an uplift episode due to the lack of ground elevation measurements.

4. Statistical analysis

To assess if the inferred association between earthquakes and bradyseismic episodes is statistically verifiable we carried out a binomial test to investigate the null hypothesis that uplift events are unrelated to earthquakes. To conduct the statistical study we considered both regional and teleseismic earthquakes. For the regional earthquakes we had to exclude fore- and after-shocks that may bias the statistical analysis. The excluding criteria for regional earthquakes is shown in Table 1. We define a seismic sequence as the group of seismic events occurring within the estimated rupture area of the main shock (Wells and Coppersmith, 1994) as either foreshocks (up to two months before the main shock) or aftershocks (up to one year after the main shock). Then we assign the PGV imposed by the main-shock to the seismic sequence and discard the foreshocks and aftershocks in our analysis. This underestimates the total energy reaching the Campi Flegrei caldera. Next, binomial tests were used to compare with the following null hypotheses:

(a) *UL/DL onsets occurred randomly and were not related to a previous earthquake.*
(b) *UL/DL peak uplift rates occurred randomly and were not related to a previous earthquake.*

We considered five time windows 0–1 yr, 1–2 yr, 2–3 yr, 3–4 yr, and 4–5 yr before each uplift/deceleration onset/peak. We use a 1-yr time window for this study as we previously used a 1-yr moving average to build the surface elevation curve shown in Fig. 1c. The probability (p) of an earthquake occurring within these time windows is given by the number of uplift/deceleration events (14) multiplied by the duration of each time window (1 yr) divided by the length of the study (70 yr). For a 1-yr time window, this gives $p = 0.2$, i.e. there is a 20% probability of a random earthquake occurring within one of these pre-defined time windows. The probability (P) that r or more earthquakes with PGV $>$ 0.1 cm/s for regional events or PGV $>$ 0.01 for teleseismic events occurred during one of these time windows is given by:

$$P = \frac{p^n (1-p)^{(r-n)} r!}{n!(r-n)!}, \quad (1)$$

where n is the total number of earthquakes with PGV $>$ 0.1 cm/s (regional events) or PGV $>$ 0.01 cm/s (teleseismic events) that occurred during the study. It should be mentioned that in binomial tests it is possible to set any arbitrary time window that (in theory) would allow us to capture all earthquake/uplift pairs. However, the binomial test has a build-in penalty for doing so, namely if the time window is longer the p-value will increase accordingly. This is because the value of p in the equation (1) is calculated by dividing the summed length of all time windows (14×1 year) by the length of the time series (70 yr). Using the binomial test given by equation (1), we obtained the p-values (P in equation (1)) summarized in Fig. 3 and given in Table 2.

These values indicate that by using the full catalogue we could reject the null hypothesis (a) for the onset of uplift within one year of a regional earthquake (p-value 0.009) and (b) maximum rate of uplift between 2 and 3 yr after the earthquake (p-value 0.049). As mentioned above, aftershock events may bias the statistical analysis favouring an association between earthquakes and uplift events. However, even with aftershocks removed from the catalogue, we could still reject the null hypothesis for the onset of uplift occurring within one year of regional earthquakes (p-value 0.007). Using this catalogue we could no longer verify the association between regional earthquakes and the maximum rate of uplift as for the same time delay (2–3 yr) we obtain a p-value of 0.3. Null hypothesis (a) cannot be rejected ($p > 0.05$) for all other time windows.

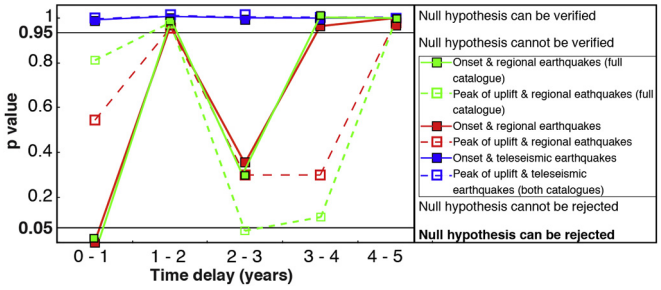

Fig. 3. Statistical study. The null hypothesis for the onset of uplift events could be rejected for the 0–1 yr time period for both catalogues (see text). Note that in binomial tests it is possible to set any arbitrary time window to try to capture all earthquake/uplift pairs. However, the binomial test has a build-in penalty for doing so: if the time window is longer, the p-value will increase accordingly. The null hypothesis for the peak of uplift events could be rejected for the 2–3 yr time period for the full catalogue and for the 2.3–3.8 yr period (not shown here) for the catalogue of Table 2. The null hypotheses for teleseismic earthquakes were all verified. (For interpretation of the colours in this figure, the reader is referred to the web version of this article.)

Table 2
Results of statistical analysis. The null hypothesis can be verified for all cases except for those that are underlined. The null hypothesis can be rejected for the case in bold text and underlined.

	0–1 yr	1–2 yr	2–3 yr	3–4 yr	4–5 yr
Binomial Test (no Aftershock considered, only the earthquakes in Table 1)					
Onset (R-EQ)	**0.007**	0.97	0.40	1	0.97
Peak (R-EQ)	0.55	0.95	0.30	0.30	1
Onset (T-EQ)	1.0	1.0	1.0	1.0	1.0
Peak (T-EQ)	1.0	1.0	1.0	1.0	1.0
Binomial Test (Full catalogue)					
Onset (R-EQ)	**0.009**	0.97	0.34	1.0	1.0
Peak (R-EQ)	0.83	0.99	**0.049**	0.12	1.0
Onset (T-EQ)	1.0	1.0	1.0	1.0	1.0
Peak (T-EQ)	1.0	1.0	1.0	1.0	1.0

For teleseismic earthquakes, all null hypotheses were statistically verified (p-value $>$ 0.99), irrespective of the choice of the parameters of the binomial test (e.g., time window and PGV threshold). The "reverse" test was also conducted, i.e. we tested the following null hypotheses:

(a) *Earthquakes occurred randomly and were not related to the onset of a future UL/DL event.*
(b) *Earthquakes occurred randomly and were not related to the peak uplift rate of a future UL/DL event.*

This test was performed by setting the number of 1-year time windows equal to the number of earthquakes and with n and r set equal to the total number of earthquakes and the number of earthquakes followed by a UL/DL event in the time window, respectively. This test gave similar results. In this case, we could still reject null hypothesis (a) (but not (b)) for regional earthquakes only. We also varied the PGV thresholds and found that our conclusion holds for PGV $<$ 0.22 cm/s for regional earthquakes and that, for teleseismic earthquakes, we cannot reject the null hypothesis regardless of our choice of PGV threshold.

We acknowledge that a p-value obtained from a statistical test is not a definitive proof that a model is valid. For example, we could consider the "opposite" (likely unphysically plausible) hypothesis i.e. that bradyseismic episodes at Campi Flegrei triggered

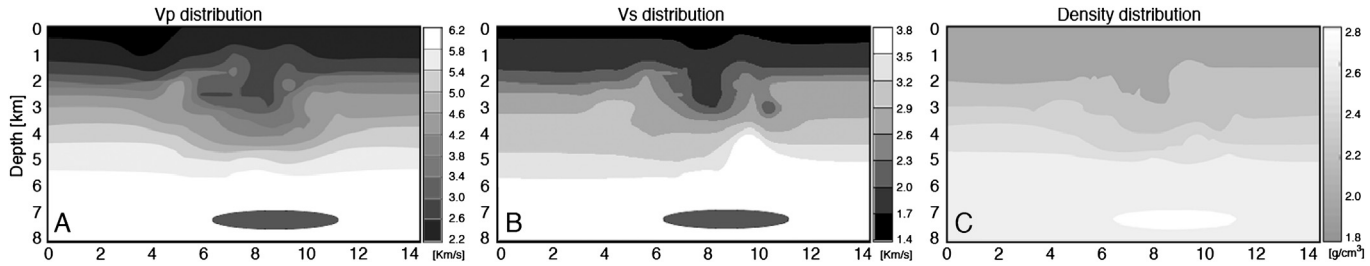

Fig. 4. Velocity and density structure of the Campi Flegrei caldera. Both the P- and S-wave velocity structure (including the magma properties) are reconstructed from tomography and seismic reflection studies of the Campi Flegrei (Vanorio et al., 2005; Zollo et al., 2008). Density variations are taken from Petrillo et al. (2013). The velocity model measures 14 × 8 km and represents a E–W profile across the caldera. The numerical model includes also the properties of the shallow hydrothermal system.

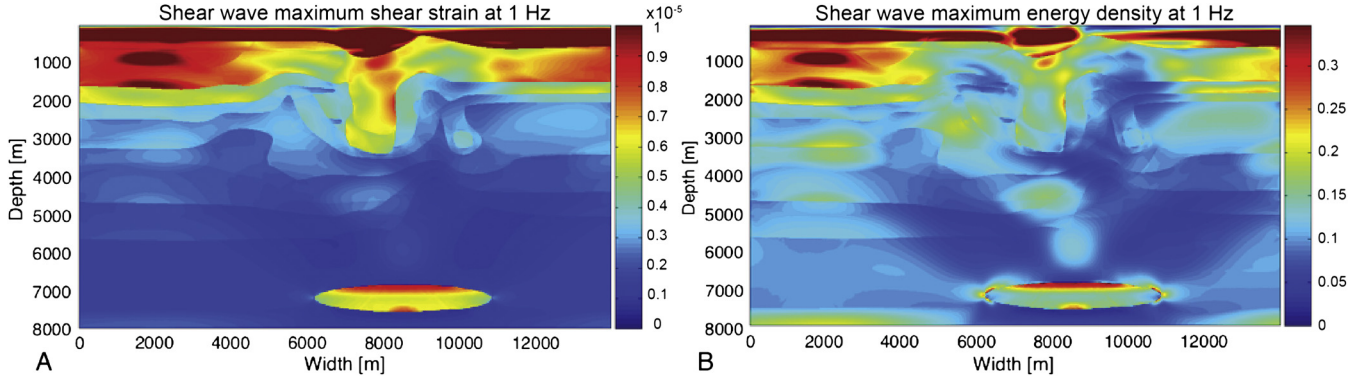

Fig. 5. Simulation results at 1 Hz for S-waves. Results are calibrated with the seismic record of the L'Aquila earthquake for 1 Hz frequency at the INGV seismic station OVO (coordinates 40.82750°N, 14.39667°E). Note that maximum values are reached at shallow depths, in the central part of the model (i.e., at 3 km depth), and at the interface between the magma chamber and the overlying host rocks. (For interpretation of the colours in this figure, the reader is referred to the web version of this article.)

earthquakes. However, by performing a similar binomial test for this hypothesis, we obtained a p-value >0.05 (0.09–0.25) for all 1-year time windows, meaning that in this case, the null hypothesis cannot be rejected. Nevertheless, because other hypotheses can exist that have not been tested in our study, we acknowledge that our statistical verification must be treated with caution.

Overall the statistical tests suggest an association between bradyseismic episodes and regional earthquakes and indicate that bradyseismic episodes are unrelated to teleseismic earthquakes. We propose that there is a causal link and that dynamic triggering is the process responsible for activating fluid release from the magmatic reservoir underlying the caldera. Dynamic triggering may impose short-lived but elevated strain rates in the far-field that are capable to promote the development of small-scale physical processes in magmatic reservoirs (Manga and Brodsky, 2006). To further investigate this hypothesis we setup numerical experiments of passing seismic waves at Campi Flegrei.

5. Numerical modelling

To identify the possible underlying mechanism for how incoming seismic energy may trigger delayed surface uplift we simulated body wave propagation through the impedance velocity structure of the Campi Flegrei (Vanorio et al., 2005; Zollo et al., 2008). The static model (Fig. 4) used for numerical seismic wave propagation modelling is based on an interpreted tomography (Vanorio et al., 2005) and a seismic reflection study (Zollo et al., 2008) and takes into account density variations (Petrillo et al., 2013). The geometry was discretized into a rotated staggered finite-difference grid of 2.5×10^7 nodes with a grid spacing of 0.675 m. We used periodic boundary conditions on the sides of the model domain and a free surface at the top of the domain. Our numerical approach is novel as we consider a high-resolution velocity model integrating a heterogeneous impedance distribution previously tested at the Lusi sediment-hosted hydrothermal system, Indonesia (Lupi et al., 2013) and at the Larderello–Travale geothermal field, Italy (Lupi et al., 2017).

The amplitude of the incoming synthetic wave is constrained such that the average vertical displacement at the surface in the simulations matches the amplitude of the recorded seismic wave that we used to calibrate the simulations. We simulate body and surface waves. P- and Love waves have weaker effects compared to S- and Rayleigh waves, respectively, and are not shown here. For body waves we assumed a central frequency of 1 Hz and for surface waves a central period of 20 s. This was because Hill (2012) shows that surface waves with central periods around 20 s may be particularly effective in pumping fluids out of magmatic reservoirs. Because the frequency of the simulated body wave is 1 Hz, we can assume that the resulting maximum absolute strain value on a specific component of the strain tensor obtained from our simulations may translate directly to strain rate values. The numerical code used in this study (Saenger et al., 2000) assumes an elastic domain. The full procedure, from discretization to model calibration is described in Lupi et al. (2013). To construct the numerical model we simplified the magmatic reservoir as an elliptical magma chamber. We calibrated the model with observed frequency contents and ground displacements caused by several earthquakes for both regional and teleseismic events. Maximum strains (Fig. 5a) generated by incident shear waves at 1 Hz (central frequency) reach 10^{-5} while energy densities (Fig. 5b) are in the order of 1 J/m^3. Seismic wave simulations using lower central frequencies (i.e., 0.5 Hz) yield lower but still significant values (i.e., maximum strains of 10^{-6}).

Simulations of Rayleigh waves with a central period of 20 s highlight that surface waves impose remarkably weaker shear strains compared to shear waves at Campi Flegrei on the deep magmatic reservoir (i.e., three orders of magnitude less) (Fig. 6). Elevated strain rates and maximum energy densities focus in regions characterized by large seismic impedance contrasts, such as the interface between the deep magmatic reservoir and the host rocks. This coincides with regions of inferred breaching of low per-

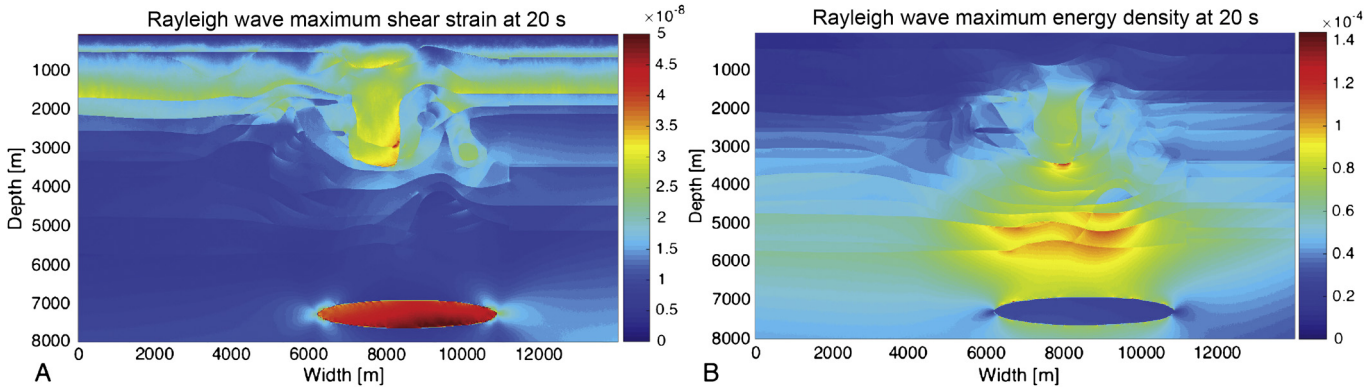

Fig. 6. Effects of Rayleigh waves with a period of 20 s at Campi Flegrei. Note that compared to Fig. 5 the values of shear strain and energy density for surface waves are three and four orders of magnitude smaller, respectively. (For interpretation of the colours in this figure, the reader is referred to the web version of this article.)

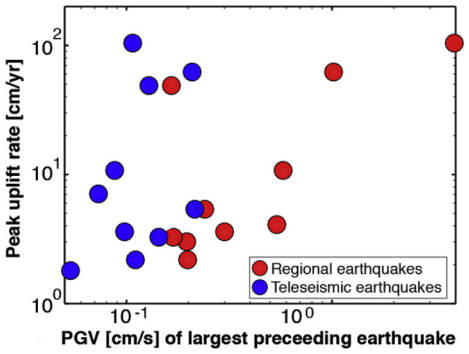

Fig. 7. Linear relationship between calculated PGV and peak uplift rate. Larger PGV promote faster uplifts for regional earthquakes. No correlation could be found for teleseismic earthquakes. The he R^2 value for a possible fitting line would be $R^2 = 0.47$ ($\log_{10}$(peak uplift rate [cm/yr]) $= 0.97 * \log_{10}$(PGV [cm/s]) $+ 1.37$). The fitting is clearly dominated by the M_w 6.9 earthquake. However, when removing this event the linear correlation still appears. (For interpretation of the references to colour in this figure, the reader is referred to the web version of this article.)

meability zones (Bodnar et al., 2007) (i.e., at ca. 3 km depth and at the top of the magma reservoir at ca. 7 km depth). According to our simulations, energy density appears to be more effectively captured when seismic waves travel from a low to a high shear wave velocity body and not vice versa. Hence, direct body waves released from regional earthquakes crossing the magma–host rock impedance contrast from below, rather than surface waves generated by teleseismic events penetrating the system from surface to depth, seem to be more effective in focusing dynamic strains at the interface between the magmatic reservoir and the host rock. This is in agreement with our statistical analysis as at short epicentral distances (i.e., for regional earthquakes) PGV is principally caused by body waves (Kulhánek, 2002).

6. Discussion

The ground at Campi Flegrei undergoing bradyseism is constantly in motion with either uplift or deflation dominating the temporal evolution (Fig. 1). Continuous monitoring allows identification of single uplift events of highly variable magnitudes, but the precise timing of onset and peak uplift is naturally blurred by the superposition of events and can only be approximated by identifying acceleration and deceleration of ground motion. Typically, the bradyseismic events indicate a delay time of about one to three years between onset and peak of uplift, followed by a longer period of deflation (Fig. 1, Table 1). A conceptual mechanistic model therefore not only has to provide a plausible explanation for the trigger but also for the intrinsic year-long timescales of ground motion and its natural variability.

In line with the variability of the delay time, our statistical analysis indicates that the relationship between regional earthquakes and onset of uplift is stronger than the relationship between regional earthquakes and peak of uplift. We further test if larger earthquakes trigger faster uplifts by plotting the peak uplift rate against PGV of all earthquake-uplift event-couples (red dots in Fig. 7), which suggests a positive correlation for the regional earthquakes, but no correlation for teleseismic earthquakes (blue dots in Fig. 7). Even though data is sparse and the correlation is dominated by a prominent earthquake-uplift couple (i.e. the M_w 6.9 Irpinia) the plot further supports a causal relationship between regional (and not teleseismic) earthquakes and uplift events.

The results of the numerical simulations indicate that the incoming seismic energy from regional earthquakes has the strongest effects at the base of the shallow hydrothermal system and at the roof of the magma chamber. The wave-induced short-lived dynamic strain rates localized at approximately 7 km depth (Fig. 5) can temporarily induce embrittlement in regions of otherwise hot ductile rocks around the magma chamber. The ductile yield curve can be approximated (Fournier, 1999) as:

$$\dot{\varepsilon} = A(\sigma_1 - \sigma_3)^n \exp\left[-Q/(RT)\right], \tag{2}$$

where $\dot{\varepsilon}$ is strain rate, R the universal gas constant, $\sigma_1 - \sigma_3$ the differential stress affecting the media, T temperature, n the stress exponent, and Q (activation energy) and A coefficients representing the type of lithology. As A, n, Q, R, and T are constant at a given point in the system, the passing wave induces increased strain rates and higher differential stresses ($\sigma_1 - \sigma_3$) shifting the ductile yield curve to greater depths (Fig. 8a). This creates a short-lived (co-seismic) brittle region (red region in Fig. 8b) within the otherwise ductile domain. The resulting failure taps the reservoir of accumulated magmatic fluids (Fig. 8c).

In this work we assume that dynamic and static stress triggering are linked to short-lived (i.e. associated to passing seismic waves) and long-lasting (i.e. shear, normal and coulomb) stresses imposed by fault slips, respectively. Previous models discussing dynamic triggering of volcanic systems suggest that the effects of passing seismic waves may promote several mechanisms eventually capable of initiating pressure build up in the magmatic reservoir and ultimately prompting to a volcanic eruption. Namiki et al. (2016) point out that passing seismic waves may promote sloshing of a bubbly magma reservoir. Manga and Brodsky (2006) provide a comprehensive review of such processes suggesting that rectified diffusion and advective overpressure may lead to pressurization of the magmatic reservoir. Watt et al. (2009) considered the role that such mechanisms may have had on the reactivation of Andean volcanoes after mega-thrust earthquakes and point out, in agreement with Pyle and Pyle (1995), that such processes cause

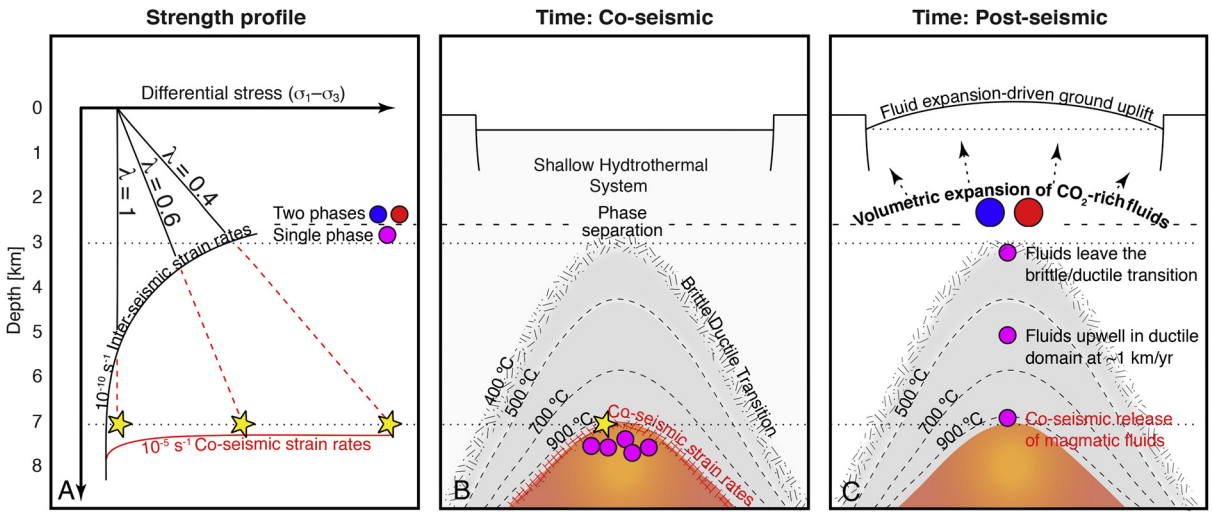

Fig. 8. Conceptual model illustrating the effects of large earthquakes at the Campi Flegrei caldera. A) Strength-vs.-depth profile for various fluid factors (λ). λ is the ratio between pore fluid pressure and overburden stress. The intersection between the brittle yield curve (diagonal lines) and the ductile yield curve (curved lines) marks the brittle/ductile transition. Inter- and co-seismic times are marked in black and red, respectively. The incoming seismic waves impose local and temporarily high strain rates of ca. 10^{-5} s^{-1}. Yellow stars indicate regions of embrittlement for different λ. B) Localization of high strains at the roof of the magma chamber promotes the release of single-phase magmatic fluids (purple circles) that subsequently flow through the ductile domain maintaining a quasi-constant volume. C) Upwelling fluids undergo phase separation (red and blue circles) and volumetric expansion at the base of the hydrothermal system (For interpretation of the references to colour in this figure legend, the reader is referred to the web version of this article.).

pressure variations that are too small to promote volcanic unrest. The short-lived brittle behaviour of otherwise ductile media introduced here and previously postulated by Fournier (1999) and simulated by Weiss et al. (2012) may be key to promote to the pressure variations necessary to mobilize magmatic fluids and lead to volcanic unrest.

Walter and Amelung (2007) show that static stress triggering imposed by middle to large magnitude earthquakes may reactivate volcanoes in the near-field since static stress triggering operates at the fault length scale (Toda et al., 2011). For the cases presented here, although static Coulomb stresses cannot be ruled out for the 1980 M_w 6.9 Irpinia earthquake, we propose that static stress variations imposed by 11 out of 12 earthquakes do not impose significant stress variations at Campi Flegrei because the epicentral distance from Campi Flegrei is too large. Conceptual models investigating (mega-thrust) earthquake–volcano interactions (Hill et al., 2002; Marzocchi, 2002) also point out that the viscoelastic relaxation of the upper lithosphere induced by the seismic slip may promote the release of magmas from the upper mantle that will ultimately replenish crustal magmatic reservoirs. However, such processes are suggested to operate over much larger time scales (i.e. from few decades to centuries). Fig. 2, available INGV online reports (INGV October Report, 2016) and Gresse et al. (2016) suggest that passing seismic waves have quasi-immediate effects on the shallow hydrothermal system of the Campi Flegrei. Recent studies (Revil et al., 2011; Vargas et al., 2017) have shown that the upper part of magmatic reservoirs and the overlaying hydrothermal systems of volcanoes are intimately connected. A seismically-triggered depressurization of the shallow hydrothermal reservoir may affect the pressure distribution of the magmatic reservoir promoting the upwelling of deeper fluids marked by prominent magmatic signatures.

Fournier (1999) and more recent numerical simulations for ore-forming magmatic-hydrothermal systems (Weis et al., 2012) suggest that the released magmatic fluids can rapidly ascend through a hot, nominally ductile region with lithostatic fluid pressure above the magmatic reservoir. The timescale of the vertical ascent of overpressured fluids from the magma reservoir depends on the amount of permeability increase due to hydraulic fracturing, which is not trivial to constrain. Numerical modelling of fluid release in porphyry copper systems suggest that permeability increase and flow rates depend on the amount of overpressured fluids, which in turn depends on the release rate from the magma chamber, attaining velocities in the order of km/yr (Weis et al., 2012). The numerical model further suggests that once the fluids are released, they will continue ascending as pulses of overpressured fluids invoking upward-moving permeability-creating fracturing events. Permeability estimates in response to major earthquakes indicate that even higher flow rates can be temporarily obtained in even deeper crustal levels. The inferred process of fluid ascent will naturally also depend on the state of the magmatic system, in particular on the availability of fluids during the seismic (triggering) event. On the other hand, events of fluid release may also be caused by the evolution of the magmatic system itself and therefore do not require an external trigger. The inferred process would therefore also be consistent with missing earthquake-uplift couples and variable onset-to-peak delay times.

Supercritical H_2O–CO_2 mixtures with compositions observed at Campi Flegrei fumaroles (Chiodini et al., 2003, 2012, 2016) will remain at near constant density of ca. 0.5 g/cm^3 during ascent through the lithostatically pressured region. The time lags identified in this study approximately represent the time necessary for the fluids to migrate from the magmatic reservoir to the top of the ductile region at Campi Flegrei located at approximately 3 km depth (Petrillo et al., 2013). There, a strong expansion is caused by phase separation of the H_2O–CO_2 fluid mixture under hydrostatic conditions (Fig. 8c).

The phase separation can efficiently impose significant uplifts as shown in previous studies (Todesco and Berrino, 2005; Hutnak et al., 2009; Chiodini et al., 2012) and, once fluid pressure is dissipated, the ground may subside again (Todesco et al., 2014). Our mechanism is in agreement with numerical models suggesting that deflation periods follow episodic fluid fluxes, possibly in conjunction with permeability and/or porosity changes due to hydraulic fracturing, fracture sealing and/or compaction of the porous media in relation to fluid-driven pressure variations (Todesco and Berrino, 2005; Hutnak et al., 2009; Chiodini et al., 2012; Todesco et al., 2014). The onset of uplift may be less affected than the peak of uplift by shallow processes that are activated by the upwelling fluids once they enter hydrothermal system (e.g., reactivation of

different fault systems, variations of permeability, slow versus fast thermal expansion), which could explain the differences in statistical relevance.

At Campi Flegrei, long-term deflation periods (e.g., 1985–2005) are suggested to be associated with compaction of the porous media driven by fluid pressure drops in the order of 1 MPa (Todesco et al., 2014). In line with these models, our mechanism infers that the onset of the deflation phase occurs when the fluid pressure induced by the expansion of the H_2O–CO_2 fluid mixture, which drives the uplift phase, is relaxed. This is due to a reduced provision of fluids from depth and the contemporaneous fluid release from the shallow hydrothermal system (which increases from approximately 3400 ton/day during deflation periods to approximately 12000 ton/day during uplift events (Todesco and Berrino, 2005).

Our model is also in agreement with recent findings of Chiodini et al. (2016)) pointing out that magmatic volatiles released by magmatic bodies in a near-critical-state (i.e., the magmatic reservoir at 7 km depth beneath Campi Flegrei) can cause volcanic unrest. The Campi Flegrei is a system capable of retaining near-critical conditions in the shallow hydrothermal systems, and possibly at greater depths, thanks to the geotechnical properties of the shallow lithologies capable of withstanding elevated strain rates (Vanorio and Kanitpanyacharoen, 2015).

Our study points out that processes activated by passing seismic waves may become apparent long after the time span of few days commonly accepted for dynamic triggering. Previous authors (Parsons, 2005; Jagla, 2011; Shelly et al., 2011; Watt et al., 2009; Johnson and Bürgmann, 2016) pointed out that effects of passing seismic waves may become apparent beyond the commonly accepted time window of few days after the passage of the seismic waves. Although for Campi Flegrei we notice that 8 out of 12 uplift events began within 1.2 yr from the triggering earthquake, the earthquake-uplift time lag may vary. We argue that such a variable time window exists because the process of fluid release and ascent is influenced by several first-order controls such as rate of fluid exsolution from the magma, CO_2 content of the upwelling fluids, and amount of permeability increase during fluid ascent. Additionally, volcanic systems are geological environments with non-linear behaviour undergoing inflation and deflation phases, implying that the preparedness of the volcanic system may vary over time. Watt et al. (2009) indicate that the response of Andean volcanoes to mega-thrust earthquakes is strongly controlled by the preparedness of the volcanic complex. Vargas et al. (2017) show how the physical state of the hydrothermal and magmatic system of the Nevados del Ruiz, Colombia, changed over 20 yr. The Campi Flegrei may have undergone similar variations over the last 70 yr resulting in a continuous variation of the physical state of its hydrothermal and magmatic system, and hence its preparedness to dynamic triggering. This may play a key role in explaining the time-variations in the response timespans shown in Table 1 (and in Fig. S1 in the supplemental material). The comparatively low occurrence of large magnitude regional earthquakes hampers the strength of statistical correlation, which is not favoured by the two different types of dataset that we correlate. However, the strong qualitative observations and the quantitative analysis (in particular for the post-1990 period) strongly support the temporal relationship between seismic events and maximum vertical uplift rates.

This manuscript proposes a provocative idea relating earthquakes and uplift events. Further studies will be needed for verification and quantification of the model, which has the potential to become a valuable observation for risk mitigation plans. More generally, if our model is correct, the timescales of uplift could provide natural evidence reflecting fluid flow processes in magmatic-hydrothermal systems.

7. Conclusions

Comparing data sets of ground deformation at Campi Flegrei, Italy, with catalogues of regional and teleseismic earthquakes suggests an association between the dynamic stresses imposed by passing body (and not surface) waves released by regional earthquakes and delayed ground uplift at the Campi Flegrei. We argue that this association (supported by yet non-definitive binomial tests) represents a causal link, which can be explained by dynamic triggering of the magmatic-hydrothermal system. These events may lead to episodic embrittlement of nominally ductile regions and subsequent release of fluid or magma from the reservoir, which eventually become the driver for ground uplift upon ascent. This model implies that the response will depend on the preparedness of the magmatic-hydrothermal system and that the timescales and magnitudes of ground deformation are subject to feedbacks between several geological processes, naturally making the proposed causative relation hard to decipher.

The Campi Flegrei is an exceptionally well-documented caldera with a long monitoring period, but with time and with the improvement of measuring techniques, it will be possible to test our proposed hypothesis at other calderas worldwide. Understanding the geological processes triggering ground deformations is key for risk assessment of volcanic hazards and more generally can provide valuable insights into processes of fluid migration at several kilometres of crustal depth at physical conditions representative of the brittle–ductile transition, which are also relevant for geothermal resources and the formation of hydrothermal ore deposits.

The most provocative (and possibly challenging) aspect of this study is the delayed response of Campi Flegrei. This study shows that uplift events at Campi Flegrei may be observed up to several months after a given earthquake. The corollary is that passing dynamic stresses may activate geological processes that can only be observed long after the few-days long time window commonly proposed for dynamic triggering. For the specific case of the Campi Flegrei we suggest that passing seismic waves focus dynamic shear strains where impedance contrasts occur, namely at the interface between fluid-saturated regions (i.e. hydrothermal and magmatic reservoirs) and the host rocks. For instance, in magmatic reservoirs such regions are often described as crystal-rich mush-like volumes in a near-critical state where fluids are trapped. Dynamic stresses may be able to promote brittle failure in these domains releasing the otherwise confined fluids. This results in crustal fluid flow that ultimately drives the observed ground uplifts. Our work point out that disturbance of the magmatic systems, not necessarily directly causing immediate eruptions, could be a much more widespread process than currently believed.

Acknowledgements

Donat Fäh is thanked for suggesting the ground motion classification of the earthquakes. Nima Riahi, Jean-Pierre Burg, and Stephen A. Miller for discussion of the paper. Andrea Parmigiani is thanked for extensive discussion on magmatic reservoirs. Matteo Lupi thanks SCCER-SoE and the Swiss National Science Foundation for financial support (grant n° PZ00P2_154815 and grant n° PYAPP2_166900). Finally, we thank the Editor, two anonymous Reviewers and Roland Bürgmann who provided constructive suggestions that improved very much the manuscript.

Appendix A. Supplementary material

Supplementary material related to this article can be found online at http://dx.doi.org/10.1016/j.epsl.2017.07.006.

References

Acocella, V., Di Lorenzo, R., Newhall, C., Scandone, R., 2015. An overview of recent (1988 to 2014) caldera unrest: knowledge and perspectives. Rev. Geophys. 53, 896–955. http://dx.doi.org/10.1002/2015RG000492.

Agnew, D.C., Wyatt, F.K., 2014. Dynamic strains at regional and teleseismic distances. Bull. Seismol. Soc. Am. 104, 1846–1859. http://dx.doi.org/10.1785/0120140007.

Amoruso, A., Crescentini, L., Sabbetta, I., De Martino, P., Obrizzo, F., Tammaro, U., 2014. Clues to the cause of the 2011–2013 Campi Flegrei caldera unrest, Italy, from continuous GPS data. Geophys. Res. Lett. 41. http://dx.doi.org/10.1002/2014GL059539.

Battaglia, M., Troise, C., Obrizzo, F., Pingue, F., De Natale, G., 2006. Evidence for fluid migration as the source of deformation at Campi Flegrei caldera (Italy). Geophys. Res. Lett. 33.

Bindi, D., Pacor, F., Luzi, L., Puglia, R., Massa, M., Ameri, G., Paolucci, R., 2011. Ground motion prediction equations derived from the Italian strong motion database. Bull. Earthq. Eng. 9, 1899–1920. http://dx.doi.org/10.1007/s10518-011-9313-z.

Bodnar, R.J., Cannatelli, C., De Vivo, B., Lima, A., Belkin, H.E., Milia, A., 2007. Quantitative model for magma degassing and ground deformation (bradyseism) at Campi Flegrei, Italy: implications for future eruptions. Geology. http://dx.doi.org/10.1130/G23653A.1.

Chiodini, G., Todesco, M., Caliro, S., Del Gaudio, C., Macedonio, G., Russo, M., 2003. Magma degassing as a trigger of bradyseismic events: the case of Phlegrean Fields (Italy). Geophys. Res. Lett. 30.

Chiodini, G., Caliro, S., De Martino, P., Avino, R., Gherardi, F., 2012. Early signals of new volcanic unrest at Campi Flegrei caldera? Insights from geochemical data and physical simulations. Geology 40, 943–946. http://dx.doi.org/10.1130/G33251.1.

Chiodini, G., Paonita, A., Aiuppa, A., Costa, A., Caliro, S., De Martino, P., Acocella, V., Vandemeulebrouck, J., 2016. Magmas near the critical degassing pressure drive volcanic unrest towards a critical state. Nat. Commun. 7, 13712. http://dx.doi.org/10.1038/ncomms13712.

De Martino, P., Tammaro, U., Obrizzo, F., 2014. GPS time series at Campi Flegrei caldera (2000–2013). Ann. Geophys. 57. http://dx.doi.org/10.4401/ag-6431.

De Natale, G., Troise, C., Pingue, F., Mastrolorenzo, G., Pappalardo, L., Battaglia, M., Boschi, E., 2006. The Campi Flegrei caldera: unrest mechanisms and hazards. Geol. Soc. (Lond.) Spec. Publ. 269, 25–45.

Del Gaudio, C., Aquino, I., Ricciardi, G.P., Ricco, C., Scandone, R., 2010. Unrest episodes at Campi Flegrei: a reconstruction of vertical ground movements during 1905–2009. J. Volcanol. Geotherm. Res. 195, 48–56. http://www.emsc-csem.org/Earthquake/?filter=yes.

Fournier, R.O., 1999. Hydrothermal processes related to movement of fluid from plastic into brittle rock in the magmatic-epithermal environment. Econ. Geol. 94, 1193–1211. http://dx.doi.org/10.2113/gsecongeo.94.8.1193.

Gresse, M., Vandemeulebrouck, J., Byrdina, S., Chiodini, G., Bruno, P.P., 2016. Changes in CO_2 diffuse degassing induced by the passing of seismic waves. J. Volcanol. Geotherm. Res. 320, 12–18. http://dx.doi.org/10.1016/j.jvolgeores.2016.04.019.

Hill, D.P., 2012. Surface-wave potential for triggering tectonic (nonvolcanic) tremor-corrected. Bull. Seismol. Soc. Am. 102, 2337–2355. http://dx.doi.org/10.1785/0120120086.

Hill, D.P., Johnston, M., Langbein, J., Bilham, R., 1995. Response of Long Valley Caldera to the M = 7.3 Landers, California, Earthquake. Geophys. Res. Lett. 100, 12985–13005.

Hill, D.P., Pollitz, F., Newhall, C., 2002. Earthquake–volcano interactions. Phys. Today 55, 41. http://dx.doi.org/10.1063/1.1535006.

Hurwitz, S., Christiansen, L.B., Hsieh, P.A., 2007. Hydrothermal fluid flow and deformation in large calderas: inferences from numerical simulations. J. Geophys. Res. 112.

Husen, S., Taylor, R., Smith, R.B., Healser, H., 2004a. Changes in geyser eruption behavior and remotely triggered seismicity in Yellowstone National Park produced by the 2002 M 7.9 Denali fault earthquake, Alaska. Geology 32, 537. http://dx.doi.org/10.1130/G20381.1.

Husen, S., Wiemer, S., Smith, R.B., 2004b. Remotely triggered seismicity in the Yellowstone National Park region by the 2002 Mw 7.9 Denali Fault earthquake, Alaska. Bull. Seismol. Soc. Am. 94, S317–S331.

Hutnak, M., Hurwitz, S., Ingebritsen, S.E., Hsieh, P.A., 2009. Numerical models of caldera deformation: effects of multiphase and multicomponent hydrothermal fluid flow. J. Geophys. Res. 114, B04411. http://dx.doi.org/10.1029/2008JB006151.

INGV, 2016. Report. http://www.ov.ingv.it/ov/bollettini-mensili-campania/Bollettino_Vulcani_Campani_2016_11.pdf.

Jagla, E.A., 2011. Delayed dynamic triggering of earthquakes: evidence from a statistical model of seismicity. Europhys. Lett. 93, 19001. http://dx.doi.org/10.1209/0295-5075/93/19001.

Johnson, C.W., Bürgmann, R., 2016. Delayed dynamic triggering: local seismicity leading up to three remote $M \geq 6$ aftershocks of the 11 April 2012 M8.6 Indian Ocean earthquake. J. Geophys. Res., Solid Earth 121, 134–151. http://dx.doi.org/10.1002/2015JB012243.

Kulhánek, O., 2002. The structure and interpretation of seismograms. Int. Geophys. 81, 333–348.

Linde, A.T., Sacks, I.S., 1998. Triggering of volcanic eruptions. Nature 395, 888–890.

Lupi, M., Saenger, E.H., Fuchs, F., Miller, S.A., 2013. Lusi mud eruption triggered by geometric focusing of seismic waves. Nat. Geosci. 6, 642–646.

Lupi, M., Fuchs, F., Saenger, E.H., 2017. Numerical simulations of passing seismic waves at the Larderello–Travale Geothermal Field, Italy. Geophys. Res. Lett. http://dx.doi.org/10.1002/2016GL072417.

Macedonio, G., 2014. Sill intrusion as a source mechanism of unrest at volcanic calderas. J. Geophys. Res., Solid Earth.

Manga, M., Brodsky, E., 2006. Seismic triggering of eruptions in the far field: volcanoes and geysers. Annu. Rev. Earth Planet. Sci. 34, 263–291.

Manga, M., Brumm, M., Rudolph, M.L., 2009. Earthquake triggering of mud volcanoes. Mar. Pet. Geol. 26, 1785–1798. http://dx.doi.org/10.1016/j.marpetgeo.2009.01.019.

Marzocchi, W., 2002. Modeling the stress variations induced by great earthquakes on the largest volcanic eruptions of the 20th century. J. Geophys.

Mele, F., Marcocci, C., Moro, R., 2007. ISIDe, Italian Seismic Instrumental and parametric Data base [www document]. http://iside.rm.ingv.it (accessed 30 May 2016).

Namiki, A., Rivalta, E., Woith, H., Walter, T.R., 2016. Sloshing of a bubbly magma reservoir as a mechanism of triggered eruptions. J. Volcanol. Geotherm. Res. 320, 156–171. http://dx.doi.org/10.1016/j.jvolgeores.2016.03.010.

Parsons, T., 2005. A hypothesis for delayed dynamic earthquake triggering. Geophys. Res. Lett. 32. http://dx.doi.org/10.1029/2004GL021811.

Petrillo, Z., Chiodini, G., Mangiacapra, A., Caliro, S., Capuano, P., Russo, G., Cardellini, C., Avino, R., 2013. Defining a 3D physical model for the hydrothermal circulation at Campi Flegrei caldera (Italy). J. Volcanol. Geotherm. Res. 264, 172–182.

Prejean, S.G., Haney, M.M., 2014. Geophysics. Shaking up volcanoes. Science 345, 39. http://dx.doi.org/10.1126/science.1256196.

Pyle, D.M., Pyle, D.L., 1995. Bubble migration and the initiation of volcanic eruptions. J. Volcanol. Geotherm. Res. 67, 227–232. http://dx.doi.org/10.1016/0377-0273(94)00111-S.

Revil, A., Finizola, A., Ricci, T., Delcher, E., Peltier, A., Barde-Cabusson, S., Avard, G., Bailly, T., Bennati, L., Byrdina, S., Colonge, J., Di Gangi, F., Douillet, G., Lupi, M., Letort, J., Tsang Hin Sun, E., 2011. Hydrogeology of Stromboli volcano, Aeolian Islands (Italy) from the interpretation of resistivity tomograms, self-potential, soil temperature and soil CO_2 concentration measurements. Geophys. J. Int. 186, 1078–1094. http://dx.doi.org/10.1111/j.1365-246X.2011.05112.x.

Saenger, E.H., Gold, N., Shapiro, S.A., 2000. Modeling the propagation of elastic waves using a modified finite-difference grid. Wave Motion 31, 77–92.

Sansivero, F., Vilardo, G., De Martino, P., Augusti, V., Chiodini, G., 2012. Campi Flegrei volcanic surveillance by thermal IR continuous monitoring. In: 11th International Conference on Quantitative InfraRed Thermography. Department of Aerospace Engineering University of Naples Federico II.

Shelly, D.R., Peng, Z., Hill, D.P., Aiken, C., 2011. Triggered creep as a possible mechanism for delayed dynamic triggering of tremor and earthquakes. Nat. Geosci. 4, 384–388. http://dx.doi.org/10.1038/ngeo1141.

Toda, S., Stein, R.S., Sevilgen, V., Lin, J., 2011. Coulomb 3.3 Graphic-Rich Deformation and Stress-Change Software for Earthquake, Tectonic. and Volcano Research and Teaching – User Guide.

Todesco, M., Berrino, G., 2005. Modeling hydrothermal fluid circulation and gravity signals at the Phlegraean Fields caldera. Earth Planet. Sci. Lett. 240, 328–338.

Todesco, M., Costa, A., Comastri, A., Colleoni, F., Spada, G., Quareni, F., 2014. Vertical ground displacement at Campi Flegrei (Italy) in the fifth century: rapid subsidence driven by pore pressure drop. Geophys. Res. Lett. 41, 1471–1478. http://dx.doi.org/10.1002/2013GL059083.

Vanorio, T., Kanitpanyacharoen, W., 2015. Rock physics of fibrous rocks akin to Roman concrete explains uplifts at Campi Flegrei Caldera. Science 80, 349.

Vanorio, T., Virieux, J., Zollo, A., Capuano, P., Russo, G., de Nice, U., di Napoli, U., 2005. 3-D seismic tomography from P- and S-microearthquake traveltimes and rock physics characterization in the Campi Flegrei Caldera. J. Geophys. Res. 110, B03201.

Vargas, C.A., Koulakov, I., Jaupart, C., Gladkov, V., Gomez, E., El Khrepy, S., Al-Arifi, N., 2017. Breathing of the Nevado del Ruiz volcano reservoir, Colombia, inferred from repeated seismic tomography. Sci. Rep. 7, 46094. http://dx.doi.org/10.1038/srep46094.

Walter, T.R., Amelung, F., 2007. Volcanic eruptions following M_w9 megathrust earthquakes: implications for the Sumatra–Andaman volcanoes. Geology 35, 539–542. http://dx.doi.org/10.1130/G23429A.1.

Watt, S.F.L., Pyle, D.M., Mather, T.A., 2009. The influence of great earthquakes on volcanic eruption rate along the Chilean subduction zone. Earth Planet. Sci. Lett. 277, 399–407. http://dx.doi.org/10.1016/j.epsl.2008.11.005.

Weis, P., Driesner, T., Heinrich, C.A., 2012. Porphyry-copper ore shells form at stable pressure–temperature fronts within dynamic fluid plumes. Science 338, 1613–1616. http://dx.doi.org/10.1126/science.1225009.

Wells, D.L., Coppersmith, K.J., 1994. New empirical relationships among magnitude, rupture length, rupture width, rupture area, and surface displacement. Bull. Seismol. Soc. Am. 84, 974–1002.

Woo, J.Y.L., Kilburn, C.R.J., 2010. Intrusion and deformation at Campi Flegrei, southern Italy: sills, dikes, and regional extension. J. Geophys. Res., Solid Earth 115, 1–21. http://dx.doi.org/10.1029/2009JB006913.

Zollo, A., Maercklin, N., Vassallo, M., Dello Iacono, D., Virieux, J., Gasparini, P., 2008. Seismic reflections reveal a massive melt layer feeding Campi Flegrei caldera. Geophys. Res. Lett. http://dx.doi.org/10.1029/2008GL034242.